Carbon 110 (2016) 215–224

Contents lists available at ScienceDirect

Carbon

journal homepage: www.elsevier.com/locate/carbon

Highly concentrated amino group-functionalized graphite encapsulated magnetic nanoparticles fabricated by a one-step arc discharge method

Rui Hu [a, b], Taiki Furukawa [c], Xiangke Wang [d], Masaaki Nagatsu [a, c, e, *]

[a] Graduate School of Science and Technology, Shizuoka University, 3-5-1 Johoku, Naka-ku, Hamamatsu 432-8561, Japan
[b] Institute of Plasma Physics, Chinese Academy of Sciences, Hefei 230031, PR China
[c] Department of Engineering, Graduate School of Integrated Science and Technology, Shizuoka University, 3-5-1, Johoku, Naka-ku, Hamamatsu 432-8561, Japan
[d] School of Environment and Chemical Engineering, North China Electric Power University, Beijing 102206, PR China
[e] Research Institute of Electronics, Shizuoka University, 3-5-1 Johoku, Naka-ku, Hamamatsu 432-8561, Japan

ARTICLE INFO

Article history:
Received 27 June 2016
Received in revised form
1 September 2016
Accepted 4 September 2016
Available online 7 September 2016

ABSTRACT

In this work, we apply a one-step direct current arc discharge method to synthesize graphite-encapsulated magnetic nanoparticles functionalized with a high concentration of amino groups uniformly without further modification or any other pre/post-treatment procedures. The synthesis was accomplished by adding different molar ratios of NH_3 into He/CH_4 gas mixture under various gas pressures. The optimized number of functionalized amino groups is evaluated to be ~3.22×10^5 per nanoparticle prepared at 50 Torr with 0.1% of NH_3. As the molar ratios of NH_3 decrease from 1.0% to 0.1%, the optical emission peaks of CN and NH are intensified gradually, and the surface structural integrities also increase. These results indicate that NH_3 not only provides -NH or $-NH_2$ fragment species to introduce amino groups incorporating with the dangling bonds activated by H radicals, but also constructs networks to flatten the outmost graphitic surfaces of encapsulated nanoparticles. As the working gas pressure changes from 25 to 100 Torr, the outmost shells formed by the dissociated CH_4/NH_3 molecules tend to be relatively less disordered.

1. Introduction

Magnetic nanoparticles are of great interest and have wide potentials in various disciplines, including magnetic resonance imaging [1], catalysis [2], biomedicine [3], environmental remediation [4], data storage [5], and magnetic fluids [6], etc. However, an inevitable problem associated with the nanosized metallic particles is their instability over long periods. The highly active non-encapsulated magnetic nanoparticles tend to be easily oxidized in air, eroded by acid/base and agglomerated to reduce their surface energy. To overcome these limitations, the development of a protective shell to isolate the metallic core against the environment is of crucial importance, and a series of strategies have been utilized using a range of coating materials, such as silica [7,8], carbon [9] and organic surfactant polymers [10,11].

Recently, carbon encapsulated magnetic nanoparticles are receiving more attention due to their much higher chemical and thermal stability as well as biocompatibility of carbon-based materials [12,13]. The encapsulated carbon shells can not only avoid the direct exposure of magnetic core and preserve the structural and interfacial stabilization of magnetic nanoparticles, but also be applied for further functionalization with specific components (e.g., functional groups, various drugs and catalytic species). Surface modification with functional groups (e.g., amino and carboxyl groups) is quite attractive for the practical applications of magnetic nanoparticles, because hydrophilic amino-functionalized carbon shells endow better dispersibility and stability. Accordingly, many approaches such as thermal decomposition [14], solvothermal process [15], micro-emulsion [16] and co-precipitation [17] have been exploited to fabricate amino-functionalized magnetic nanoparticles. However, rigorous reacting conditions, toxic reactants and difficulties in terms of liquid waste greatly limit their practical

* Corresponding author. Graduate School of Science and Technology, Shizuoka University, 3-5-1 Johoku, Naka-ku, Hamamatsu 432-8561, Japan.
E-mail address: tmnagat@ipc.shizuoka.ac.jp (M. Nagatsu).

http://dx.doi.org/10.1016/j.carbon.2016.09.008
0008-6223/

applications. The dry plasma treatment would be an environmentally friendly method with a short processing time, and is also able to provide various functional groups [18].

Since then, many researchers focus on the fabrication and surface functionalization of metallic nanoparticles by a plasma processing. As reported in our previous papers [19–21], we have successfully fabricated graphite-encapsulated magnetic nanoparticles (GEMNPs) and graphite-encapsulated gold nanoparticles by a direct current (DC) arc discharge method and functionalized their surfaces with amino groups by applying radio frequency inductively-coupled plasma. During the processing, the nanoparticles were dispersed onto the sample stage as widely as possible. The uniform treatment of the entire surfaces of nanoparticles was quite difficult because the amino modification would only occur on the top side of the samples. We also greatly enhanced the surface interaction between GEMNPs and activated species of plasma by employing the particle explosion where the nanoparticles were ion-sputtered via a negative pulsed biasing of the sample stage during the plasma treatment [21]. However, sputtered magnetic nanoparticles would be agglomerated and still less exposed to the plasma. The fabrication of GEMNPs functionalized by amino groups uniformly using a plasma technique is one of the challenges in this field. The motivation of our research stems from the need for direct fabrication of amino-functionalized GEMNPs by a one-step plasma synthetic process.

In this paper, the fabrication of highly-concentrated amino-functionalized GEMNPs is reported via a one-step DC arc discharge method. We quantify the number of modified amino groups, and focus on the surface morphological and structural analysis of the as-prepared GEMNPs by scanning transmission electron microscopy (STEM) and Raman spectroscopy. The influences of molar ratios of NH_3 in the gas mixture and the working gas pressures on the surface morphology and the number of amino groups are discussed thoroughly.

2. Experimental

2.1. Materials

Iron oxide powder (99.99%) and graphite powder (99.99%) were purchased at New Metals and Chemicals Ltd. graphite rod (99.99%) at Nilaco Corporation, and Graphibond™ 551-R at AMECO Corporation, respectively. All the chemicals and solvents were used without any further purification.

2.2. Fabrication of amino-functionalized GEMNPs

The amino-functionalized GEMNPs were fabricated using a DC arc discharge method. Two graphite rods (50 mm × Ø10 mm) were set inside the stainless-steel chamber. A hole of around 8 mm in diameter and 15 mm in depth was drilled in the center of the graphite rod. The hole was filled with a mixture of iron oxide powder, graphite powder and graphibond with an initial mass ratio of 1:1:2. The cathode was a pointed graphite rod. Then the whole system was evacuated to several Pa by a rotary pump. A mixture gas of $He/CH_4/NH_3$ with specific molar ratios was backfilled as the reactant gas to the chamber until the pressure reached specific pressures. The molar ratio of He/CH_4 was kept as 4:1 in all these experiments. The distance between two rods could be adjusted by a linear motion feedthrough with a micrometer head outside of the chamber to control the discharge process. The arc discharge was generated by applying a high direct current of 120 A and a potential of 20 V between the two electrodes. The duration of the DC arc discharge was controlled to be 20 s. The directly deposited powders on the thin tantalum sheet substrates located at 10 cm upward in a vertical direction from the central axis of electrodes were collected. Considering the different molar ratios of NH_3 in the gas mixture and different working gas pressures, we termed the samples as GEMNPs-xNH_3 (x: the molar ratio of NH_3, at 100 Torr) and GEMNPs-y (y: the working gas pressure in unit of Torr, with 0.1% of NH_3).

2.3. Characterization

STEM analysis was performed on JEM-2100F (JEOL) instrument operated at the beam energy of 200 kV. X-ray diffraction (XRD) analysis was measured on RINT Ultima II (Rigaku) equipped with Cu Kα radiation (λ = 0.15406 nm). Raman spectra were recorded on NRS-103 7100F (JASCO) at the excitation wavelength of 532 nm. X-ray photoelectron spectroscopy (XPS) measurements were conducted with an ESCALAB Mark II system (VG Scientific). Optical emission spectroscopy (OES) measurement was performed by means of an USB2000+ (Ocean Optics) Miniature Fiber Optic Spectrometer. The optical fiber was collimated and placed directly above the discharge center (24 cm to the center). As for the quantitative analysis of amino group population introduced onto the GEMNPs, we used a conventional chemical derivatization method using the UV–Vis absorption spectroscopy with an Infinite 200 Pro (TECAN).

2.4. Quantification of amino groups

The quantification of modified amino functional groups was analyzed through the chemical derivatization method by employing sulfosuccinimidyl 6-[3′(2-pyridyldithio)-propion-amido] hexanoate (sulfo-LC-SPDP) according to the specific chemical procedures [22,23]. 250 μg of amino-functionalized GEMNPs were well dispersed into 200 μL of 10 mM sulfo-LC-SPDP in phosphate buffer saline (PBS) and reacted for 30 min under a dark condition with a ultrasonication of each 5 min. Then reacted GEMNPs were rinsed with PBS thoroughly. After that, GEMNPs with sulfo-LC-SPDP complexes were reacted with 300 μL of 20 mM dithiothreitol in PBS under dark condition. After a 15 min reaction, the nanoparticles were separated by centrifugation at 14000 rpm, and the cleaved product (i.e., pyridine-2-thione) liberated from the sulfo-LC-SPDP in the supernatant liquid was determined by measuring the absorbance at 343 nm using a microplate reader (Infinite 200 Pro, TECAN). The number of amino groups in 250 μg of amino-functionalized GEMNPs was quantitatively determined from the calibration curve using the extinction coefficient of pyridine-2-thione at 343 nm (i.e., 8.08×10^3 M^{-1} cm^{-1}). The number of nanoparticles per gram was calculated to be 1.14×10^{14} by assuming that the nanoparticles have a regularly spherical shape with roughly 20 nm of average core diameter determined from the nanoparticle size distribution taken by high resolution transmission microscopy (HRTEM). Then the number of amino groups modified on the surface of one nanoparticle could be evaluated.

3. Results and discussion

3.1. Characterization of amino-functionalized GEMNPs

Fig. 1a shows that the as-prepared GEMNPs-0.1%NH_3 are quasi-spherical in shape, and magnetic cores are clearly encapsulated by graphitic carbon layers as the fine lattice fringes exhibited (i.e., 0.338 nm of graphite (002), 0.203 nm of α-iron (110) or Fe_3C (031)). The size distribution of amino-functionalized GEMNPs-0.1%NH_3 is determined from multiple STEM images. As shown in Fig. 1b, the average nanoparticle diameter and shell thickness of amino-functionalized GEMNPs with a standard deviation are

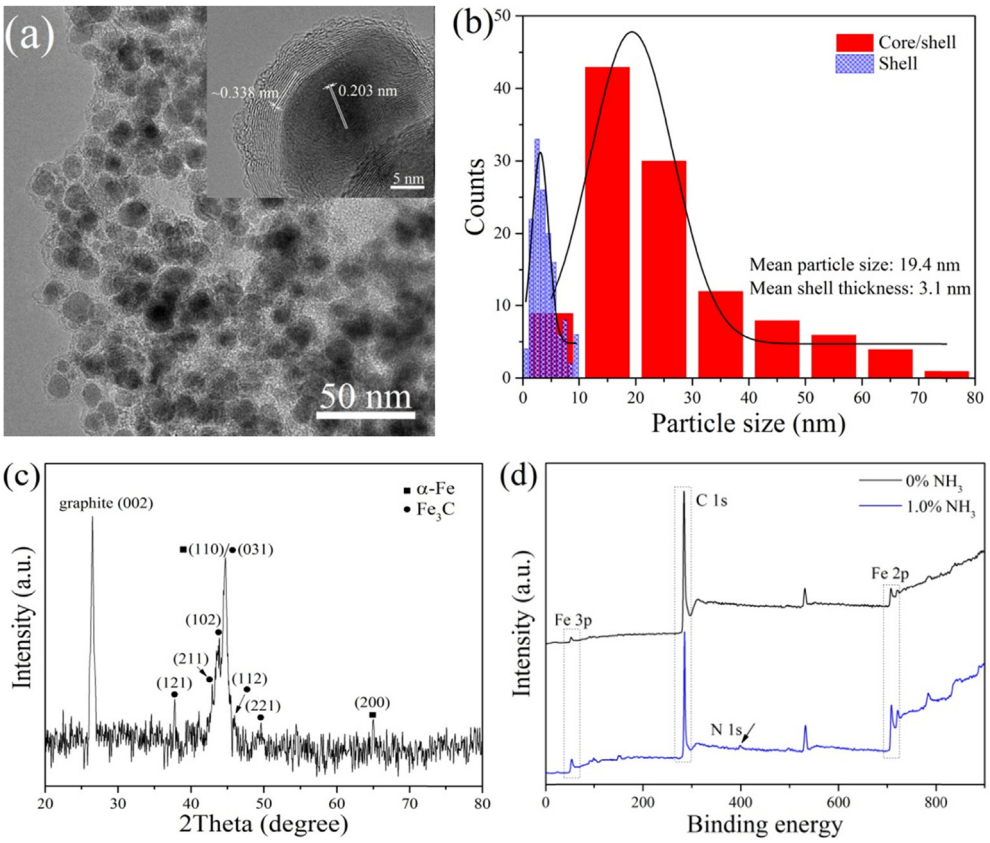

Fig. 1. Characterization of amino-functionalized GEMNPs. (a) Typical STEM image (inset: HRTEM image showing the fine lattice structure); (b) size distribution curves of shell thickness and nanoparticle diameter; (c) XRD pattern; (d) XPS survey scans of GEMNPs-0%NH_3 and GEMNPs-1.0%NH_3. (A colour version of this figure can be viewed online.)

19.4 ± 1.7 nm and 3.1 ± 0.2 nm, respectively. The crystalline structure of GEMNPs was studied using XRD technique as shown in Fig. 1c. The narrow and sharp peak at $2\theta = 26.5°$ attributed to the (002) reflection of graphitic carbon is unambiguously observed. The diffraction peaks at 37.9°, 42.9°, 43.7°, 44.7°, 46.0° and 49.6° can be ascribed to the (121), (211), (102), (031), (112) and (221) crystal reflections of Fe_3C (JCPDS 01-072-1110), respectively. Peaks at 44.7° and 65.9° are corresponded to the (110) and (200) reflections of α-Fe (JCPDS 00-006-0696), respectively. This result indicates Fe_3C and α-Fe coexist in the as-prepared GEMNPs, which are related to the reduction phase transformation of iron oxide during the arc discharge, i.e., $Fe_2O_3 \rightarrow Fe_3O_4 \rightarrow FeO \rightarrow Fe \rightarrow Fe_3C$ [24,25]. Moreover, XPS measurements were also conducted to analyze the surface property of GEMNPs. As shown in Fig. 1d, carbon (C 1s at 284.0 eV) and iron (Fe 3p at 54.0 eV and Fe 2p at 708 eV) are exhibited in the wide-scan spectrum of GEMNPs-0%NH_3 and GEMNPs-1.0%NH_3. The clearly observation of N 1s peak demonstrates the successful modification of amino functional groups on GEMNPs-1.0%NH_3.

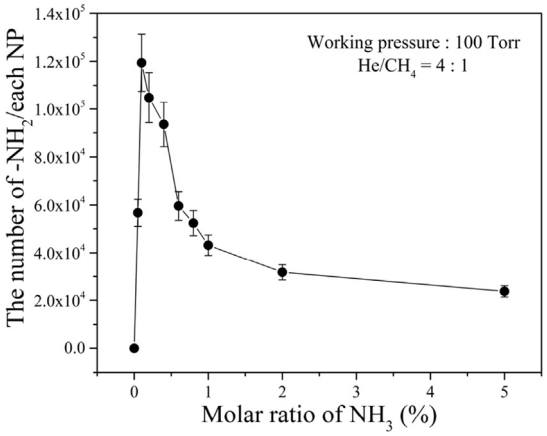

Fig. 2. Quantification of amino groups on GEMNPs prepared with different NH_3 gas mixture ratios.

3.2. Effect of the molar ratio of NH_3

The numbers of amino groups introduced on the surfaces of GEMNPs fabricated with different molar ratios of NH_3 from 0.05% to 5.0% were quantitatively evaluated by the conventional chemical protocol as described in the experimental section, and the results are shown in Fig. 2. The number of amino groups increases from zero to about 1.19×10^5 per nanoparticle as the molar ratios of NH_3 increases from 0% to 0.1%, and then reduces to 2.37×10^4 per nanoparticle as NH_3 gas mixture ratio increases to 5.0%. For the arc discharge plasma occurred at 100 Torr, both the light and heavy particles are nearly in thermal equilibrium, suggesting that the temperatures of gas molecules and electrons are approximately equal. The mainly generated processes for NH and NH_2 radicals can be attributed to the energy exchange between He metastable atoms (19.8 eV) and NH_3 molecules, and Penning excitation with subsequent dissociative recombination [26]:

$$NH_3 + He^* \rightarrow NH_2 + H + He$$
$$\rightarrow NH + H_2 + He$$
$$\rightarrow NH_3^+ + e^- + He,$$

$$NH_3^+ + e^- \rightarrow NH_2 + H,$$

where He* is the He metastable atom generated via electron collisions. As the molar ratio of NH_3 decreases from 5.0% to 0.1%, a more efficient decomposition of NH_3 in the entire arc gap may be achieved when the applied discharge power keeps constant. Hence more amino groups are functionalized on the surfaces of GEMNPs-0.1%NH_3 correspondingly.

The OES measurements were carried out to diagnose the He/CH_4/NH_3 arc discharge plasma with typical experimental conditions as shown in Fig. 3. As the molar ratio of NH_3 increases from 0% to 1.0%, similar emission spectra ranging from the wavelength of 300 nm–680 nm were governed by the optical emission of several predominant species, i.e., C_1, C_2, C_3, Fe I (excited neutral atoms) and Fe II (ions), which are coincided with previous reports [27,28]. No obvious peaks of CH electron transition ($A - X(^2\Delta - \Pi^2)$ at 431.5 nm and $B - X(^2\Sigma - ^2\Pi)$ at 387.5 nm) and atomic H (H_α at 656.5 nm, H_β at 486.1 nm) were detected in the spectrum of He/CH_4 arc plasma. The emission intensities of CH species and atomic H were extremely low while compared with the dominant existed species. It can be speculated that the graphite powder in the molded rod will act as the main carbon source in the initial stage of the arc discharge, namely, the carbon dissolved into the metallic matrix is mainly derived from the graphite powder. By adding 1.0%, 0.4% and 0.1% of NH_3 in the working gas mixture, the weak emission peaks of atomic H become visible gradually. For the spectrum of GEMNPs-0.1%NH_3, the peaks of CN ($B^2\Sigma - X^2\Sigma$ (0,0) at 388.5 nm) and NH ($A^3\Pi_{v'=0,1} - X^3\Sigma^-_{v''=0,1}$ at 336.0 nm) are both clearly exhibited, providing the existed evidence of NH_2 through the reactions of $NH_2 + He^* \rightarrow NH + H + He$ [29], even no optical emission of NH_2 species was detected. The increasing amounts of NH, CN and H radicals in the growing regime of GEMNPs will make the amino-functionalized process more effective. This is in good agreement with the quantitative result of amino groups.

Fig. 4 shows the typical HRTEM images of GEMNPs prepared with various molar ratios of NH_3 in the working gas mixture. No structural change occurs for the inner graphite layers and magnetic core, whereas the morphological differences of the outmost shells are clearly observed. For the GEMNPs-0%NH_3 (Fig. 4a and b), many carbon nano loops with a size from ~0.8 nm to ~2.0 nm are roughly distributed on the surfaces of coated shells (indicated by red arrows). While 1.0% of NH_3 is added into the gas mixture, the nano loops tend to be compressed as presented in Fig. 4c and d. For the GENMPs-0.4%NH_3 (Fig. 4e and f), the surfaces tend to be relatively less roughened without obvious nano loops located. By adding 0.1% of NH_3, the surface microstructure of GEMNPs-0.1%NH_3 (Fig. 4g and h) is of high integrity. The typical Raman spectra of GEMNPs in Fig. 5a shows that the I_D/I_G ratios of the samples prepared with different molar ratios of NH_3 from 0% to 1.0% are 0.973, 0.872, 0.884 and 0.968, respectively, indicating that the extent of defective nanostructures in GEMNPs-0.1%NH_3 is minimal. This result is consistent with the HRTEM results mentioned above.

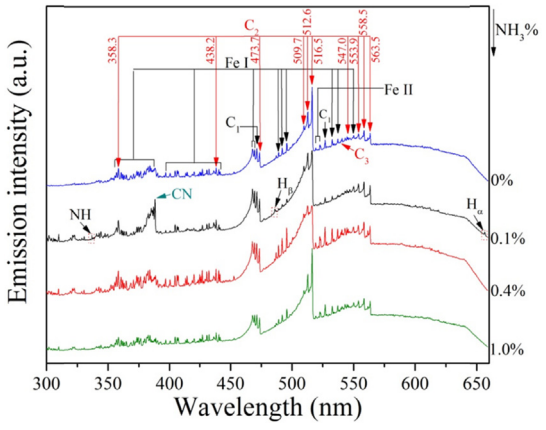

Fig. 3. Typical optical emission spectra for the DC arc discharge systems with different molar ratios of NH_3. (A colour version of this figure can be viewed online.)

Here, we will discuss about the reason why this surface morphological evolution occurs. When an arc discharge is generated between the two electrodes, the rod with iron oxide-graphite mixture will gasify immediately due to the extremely high temperature in the arc center. Carbon atoms evaporated from graphite powder will coagulate with each other to form small clusters, and dissolve into unit cells of iron clusters owing to the high carbon solubility of iron in the high temperature regime. Due to the collision with surrounding gas molecules, the temperature of nanoparticles decreases, and carbon solubility of iron will also reduce to initiate the precipitation of carbon atoms from the iron carbide matrix. As the outmost shell is formed by emerging carbon atoms, the graphitization will be initiated on the very beginning encapsulating carbon layer, and then this outer graphene layer will trap the core inside to block the graphitization of deposited carbon clusters on the surfaces of the nanoparticles. As the cooling goes on from the surface to the center of the nanoparticles, the internal carbon layers will be graphitized and grow by keeping their planes parallel to the external layer due to the catalysis of metallic core. Hence these layer-by-layered assembled GEMNPs are formed [30,31].

Meanwhile, CH_4 and NH_3 in the arc plasma regime will release dissociated H radicals to activate C-C bond so that more C/N-containing species can add to the growth of encapsulated layers. However, due to the lack of catalytic effect of metal (inactivation or poisoning by coated graphitic layers), the nanostructures formed on the outmost surfaces of coated shells are nano loops. There exists an activation barrier against the formation of compacted graphite layers from dissociated CH_4/NH_3 radicals (e.g., C_2H_2, N_2H_4) [32,33]. Given the larger bonding energy of C-C bond (345 kJ/mol) than those of C-N bond (305 kJ/mol) and N-N bond (160 kJ/mol) (i.e., stronger strength of C-C bond than those of C-N and N-N bond) [34], the energy barrier to form orderly arranged N-containing networks is lower than that of pure carbon ones. The dissociated nitrogen-containing radicals in ammonia plasma region will serve as nitrogen precursors for the nitrogen doping of GEMNPs. Here we analyze the surface doping situations of these GEMNPs. As shown in Fig. 5b and c, the N 1s region can be deconvoluted into four types, i.e., pyridinic N (398.2 eV), amino N (399.2eV), pyrrolic N (400.4 eV) and quaternary N (401.9 eV) [35]. The upward tendency of the intensities of amino N peaks from GEMNPs-1.0%NH_3 to GEMNPs-0.1% NH_3 is also in agreement with that of amino group quantification. While the molar ratio of NH_3 decreases from 1.0% to 0.1%, more dissociated H radicals are generated to etch the formed nano loops on the outer layers in the arc plasma regime, and the surfaces of GEMNPs tend to be more smooth and tidy. During this etching (by H radicals)-growing (by C/N-containing radicals) process of nano loops, the surface structural integrity evolves in the order of GEMNPs-0.1%NH_3 > GEMNPs-0.4%NH_3 > GEMNPs-1.0%NH_3, as illustrated in Fig. 5d. It is also found from optical emission spectrum shown in Fig. 3 that CN and H species are remarkably generated in case of 0.1% of NH_3 compared with other cases. Hence, NH_3 plays an important role in not only providing -NH/-NH_2 functional groups to

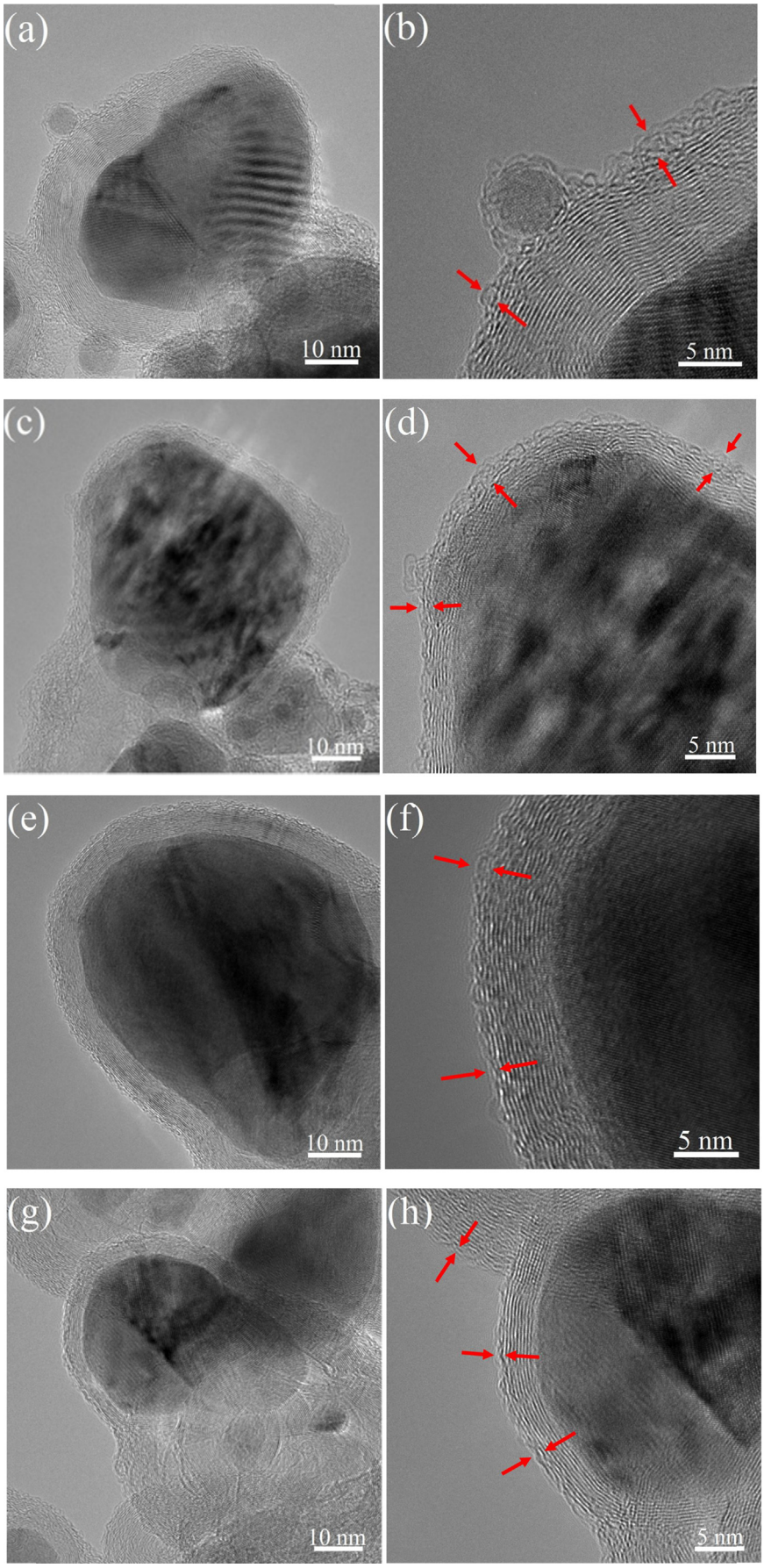

Fig. 4. STEM images of GEMNPs fabricated with different ratios of NH_3 at the working gas pressure of 100 Torr: (a, b) 0%; (c, d) 1.0%; (e, f) 0.4%; (g, h) 0.1%. (A colour version of this figure can be viewed online.)

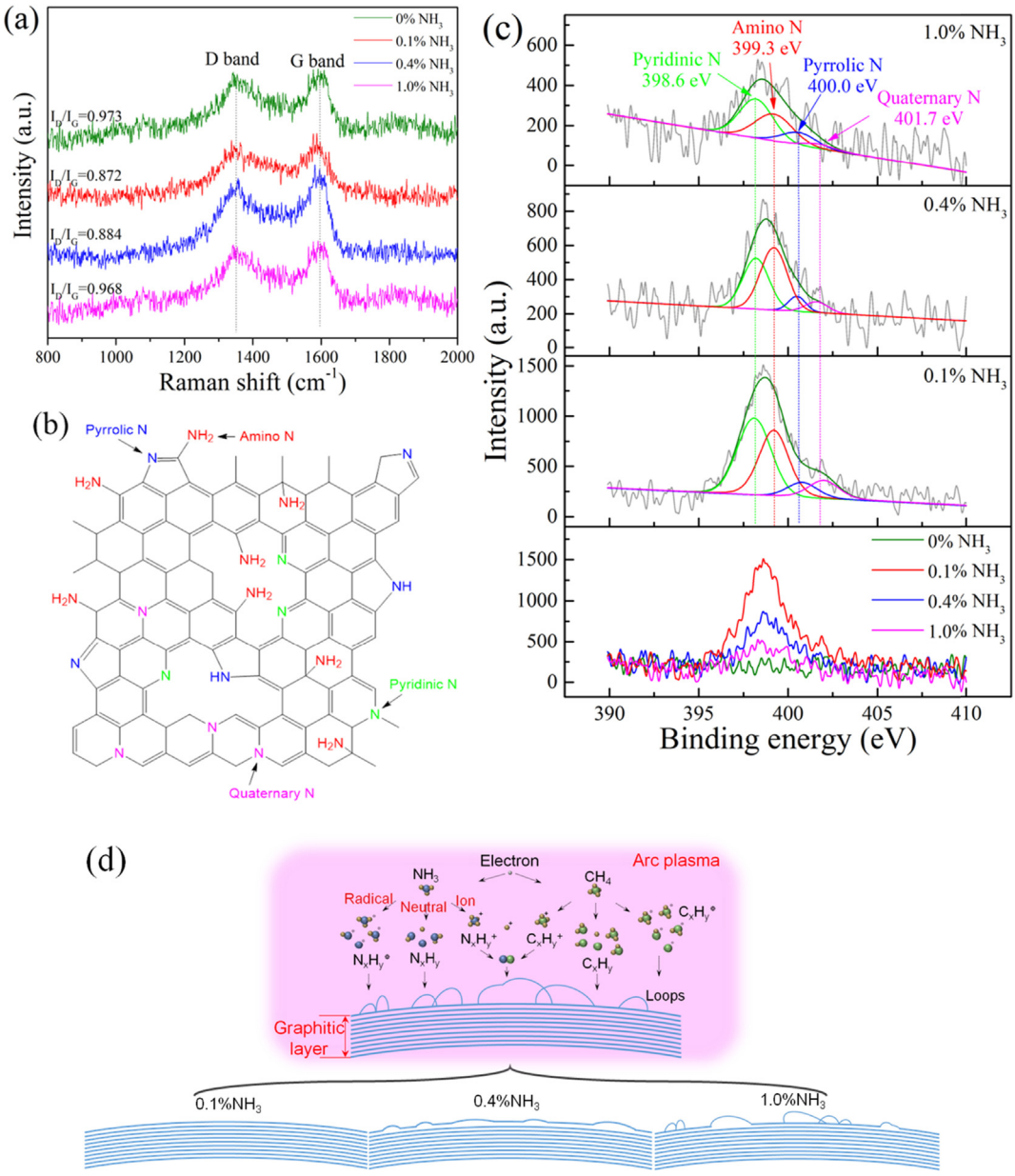

Fig. 5. (a) Raman spectra of GEMNPs-0.1%NH_3. (b) Illustration of different types of nitrogen atoms in the outmost layers of graphite shells. (c) High resolution N 1s spectra of GEMNPs. (d) Schematic showing the surface morphological evolution of GEMNPs. (A colour version of this figure can be viewed online.)

incorporate with the dangling bonds activated by H radicals, but performing the construction of networks to flatten the surfaces as well.

3.3. Effect of the working gas pressure

STEM images of amino-functionalized GEMNPs fabricated at different working gas pressures reveal that all of the as-grown GEMNPs are quasi-spherical in shape as shown in Fig. 6. By altering the working gas pressure, the average nanoparticle diameter of amino-functionalized GEMNPs with a standard deviation are 23.1 ± 3.2 nm (at 25 Torr, Fig. 6a), 21.4 ± 3.2 nm (at 50 Torr, Fig. 6b), 20.9 ± 1.4 nm (at 75 Torr, Fig. 6c) and 19.4 ± 1.7 nm (at 100 Torr, Fig. 1a), respectively.

The quantitative number of amino groups on the surfaces of GEMNPs fabricated at different working gas pressures with 0.1% of NH_3 are exhibited in Fig. 7. The optimum working gas pressure for the modification of amino groups is 50 Torr. The numbers of amino groups on the surfaces of GEMNPs-50 Torr prepared with 0.1%, 0.4% and 1.0% of NH_3 are calculated to be ~3.22×10^5, 1.42×10^5 and 7.50×10^4 per nanoparticle, respectively. It should be noted here that the maximum number of amino groups on GEMNPs-50 Torr prepared with 0.1% NH_3 addition, 3.22×10^5 per nanoparticle, is about 5 times higher than those observed in our previous study using the RF plasma surface modification with a pulsed powder explosion method [21]. In this study, it is expected that the surfaces of GEMNPs were uniformly and individually functionalized during the DC arc discharge, where the surface chemical modifications were simultaneously performed during the nanoparticle synthesis.

According to Paschen's law, the value of $p{\cdot}d$ keeps constant at the minimum of breakdown voltage. While the working gas pressure increases from 25 Torr to 100 Torr, the inter-electrode distance

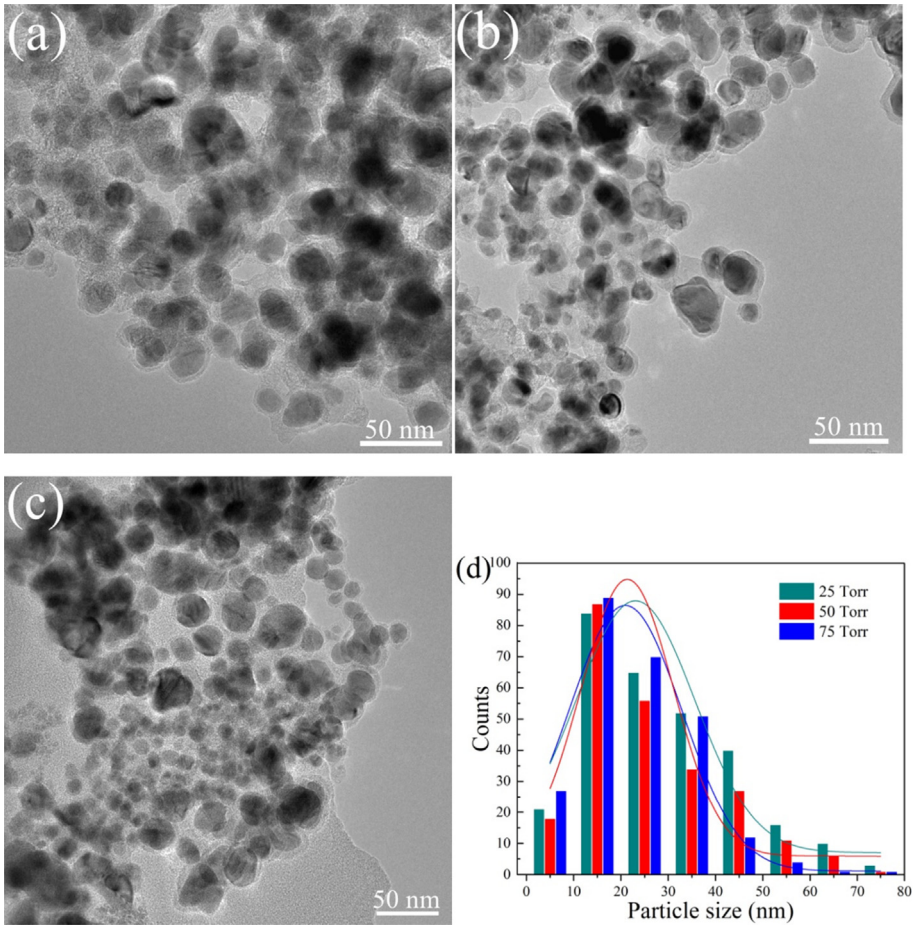

Fig. 6. STEM images of amino-functionalized GEMNPs prepared at different working gas pressures with 0.1% of NH_3: (a) 25 Torr, (b) 50 Torr, (c) 75 Torr; (d) corresponding size distribution histograms of nanoparticle diameters. (A colour version of this figure can be viewed online.)

(i.e., arc plasma size), and also mean free path of plasma species both decrease. At higher ambient pressure, the diffusion of hot species evaporated from the arc gap is restricted and the vapor is confined to a narrow region near the evaporation source. Correspondingly, the GEMNPs pass through a shorter path length of CH_4/NH_3 plasma zone, resulting in less number of amino groups modified on the carbon shells and also smaller diameter of GEMNPs due to their shorter interaction length with surrounding gas species. As a consequence, the number of grafted amino groups on GEMNPs should be in the order of 25 Torr > 50 Torr > 75 Torr > 100 Torr. However, there remains a question why the number of modified amino groups prepared at 25 Torr is less than that at 50 Torr in our experiment. At high working pressure (e.g., 75 and 100 Torr), the main approach to generate -NH and -NH_2 radicals in the thermal plasma can be attributed to the energy exchange between He metastable atoms and NH_3 molecules, and Penning excitation with subsequent dissociative recombination. However, as we described before, due to the decrease of electron mean free path, the produced He metastable atoms are limited to the arc plasma region and their production are suppressed at higher pressure. This is also the reason why fewer -NH and -NH_2 radicals are generated at higher pressure region.

On the other hand, at low working gas pressure (e.g., 25 and 50 Torr), the electron kinetic energy becomes higher than that at higher pressure due to longer electron mean free path at a given input DC voltage. Hence, He metastable atoms can be generated by

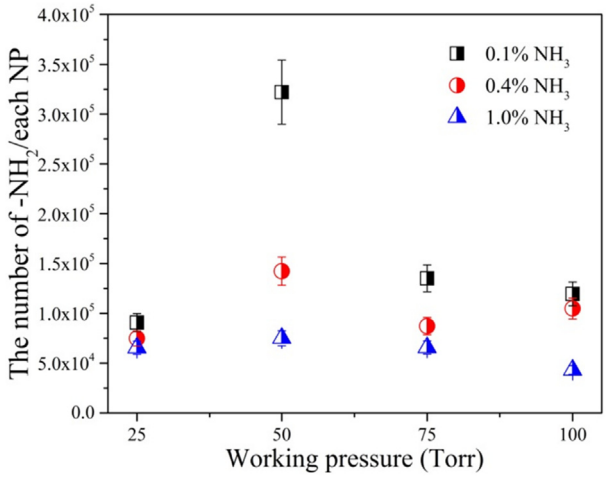

Fig. 7. Quantification of amino groups on GEMNPs prepared at different working gas pressures and NH_3 gas mixture ratios. (A colour version of this figure can be viewed online.)

electron impact excitation with He atoms, which leads to the efficient decomposition of NH_3 in the discharge gap. Therefore, as He and NH_3 gas pressure decreases, the production of -NH and -NH_2 radicals by the DC arc discharge automatically decrease. This is a plausible reason why the number of amino groups on GEMNPs

prepared at 25 Torr is lower than that at 50 Torr. Hence, given all these influential factors, the optimized working gas condition for the one-step fabrication of amino-functionalized GEMNPs by the DC arc discharge method is achieved as follows: $He/CH_4/NH_3 = 39.96$ Torr: 9.99 Torr: 0.05 Torr.

The typical surface microstructures of GEMNPs fabricated at different working pressures with 0.1% of NH_3 are observed as shown in Fig. 8. According to the indirect growth mode of GEMNPs prepared by iron group elements-carbon arc discharge method [36], the dissolved carbon re-precipitates out from the metallic matrix to form assembled graphite covers by stacking layers, which is intuitively exhibited in Fig. 8a. As the red arrows point, the re-precipitated graphite layers composed of parallel straight graphene layers are arranged orderly. It is interesting to note that the whole surface of the coating shell tends to be disorganized roughly comparing with the inner graphite layers. By the magnified observation of GEMNPs-25 Torr, one can see that the coating shell is divided into two parts distinctly: inner part composed of ordered parallel graphite layers, outer part composed of relatively disordered carbon covers with bunches (indicated inside Fig. 8b). While

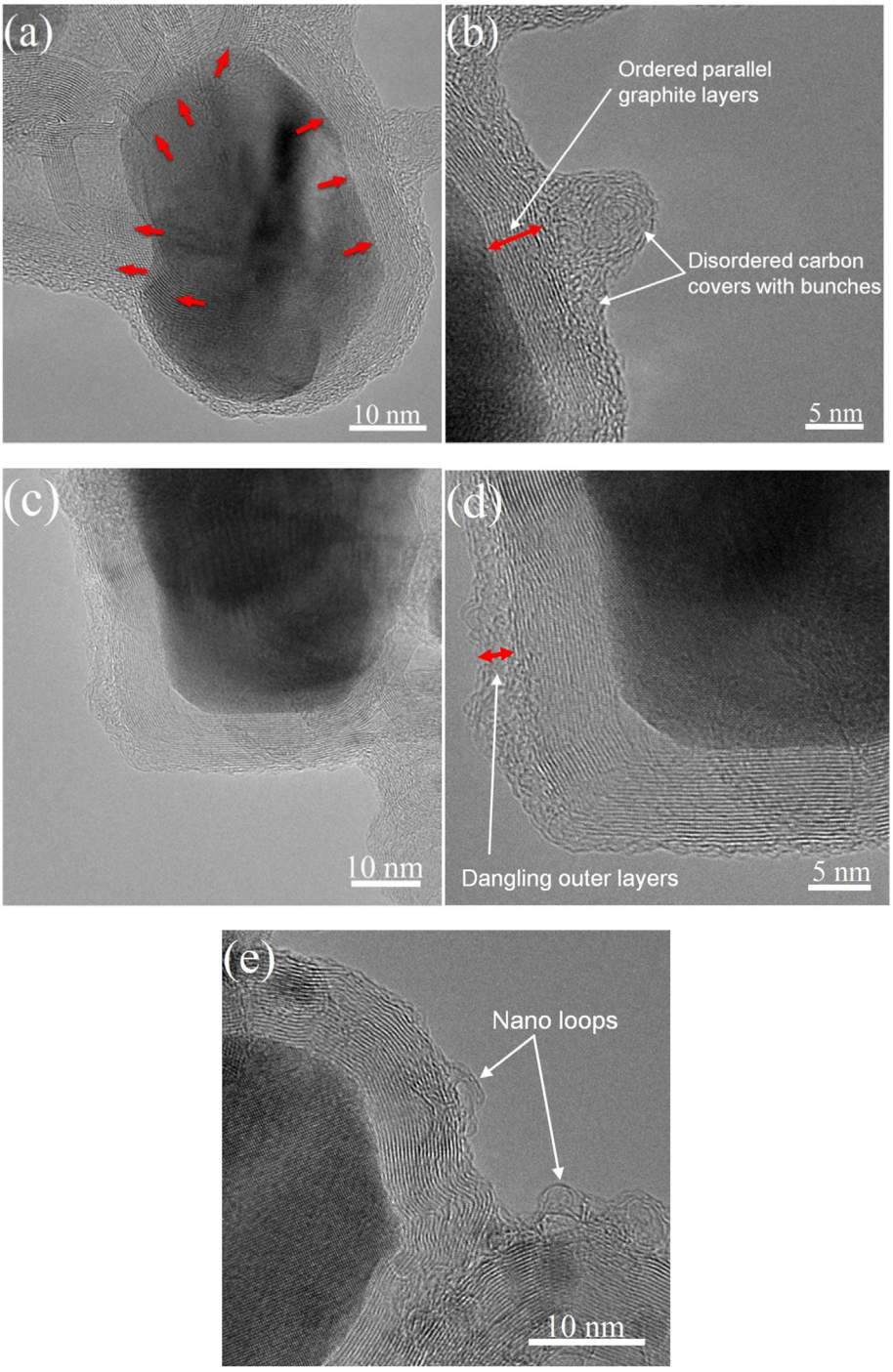

Fig. 8. Typical STEM images of GEMNPs prepared at different working gas pressures with 0.1% of NH_3: (a,b) 25 Torr, (c,d) 50 Torr, (e) 75 Torr. (A colour version of this figure can be viewed online.)

the working pressure changes to 50 Torr, the disorganized outer part is partially observed on the surfaces of GEMNPs-50 Torr (e.g., only left side of GEMNPs as shown in Fig. 8c). The entangled graphite layers are not fully compacted in this outer part, leaving some dangling positions. For the GEMNPs-75 Torr (Fig. 8e), only some nano loops are raised and located on the outmost layer of graphite shells (indicated by white arrows in Fig. 8d), and other parts of the surface are well flatted, which is quite similar to the morphology of GEMNPs-100 Torr prepared with 0.1% of NH_3 (Fig. 4h).

The gas temperature and working gas pressure cannot be controlled independently in arc plasma, namely, the decline in working gas pressure will induce a decreasing gas temperature in the nucleation and growth regime around the arc gap. Considering the existence of the activation barrier against the formation of compacted layers, at lower gas temperature and pressure, the dissociated CH_4/NH_3 molecules are arranged to form relatively disordered covers rather than parallel layers constituted of hexagons. The energy barrier makes the weak bonds between graphite-like layers cannot be formed stably, resulting in the formation of dangling covers, which are mainly composed of nitrogen doped substituent groups with relatively high molecular weights. These substituent groups would also provide much more free bonds to link with amino groups.

Assuming the integrated outmost layer of GEMNPs-0.1%NH_3 (Fig. 3g and h) is composed of pure carbon constitute, the number of carbon atoms on the outmost layer of one GMNP can be calculated as: $N_{(\text{carbon atoms})} = 2\ N_{(\text{benzene ring})} = 2S_{NP}/S_{(\text{benzene ring})}$, $S_{(\text{benzene ring})} = 3\sqrt{3}/2 \times d^2$, where $N_{(\text{carbon atoms})}$ and $N_{(\text{benzene ring})}$ are the number of carbon atoms and benzene rings on the outmost layer, respectively; d is the in-plain C-C bond length of graphite (0.142 nm) [37]; S_{NP} is the surface area of one GEMNP (radius of GEMNP = 10 nm); $S_{(\text{benzene ring})}$ is the surface area of a benzene ring. Then the calculated values of S_{NP}, $S_{(\text{benzene ring})}$ and $N_{(\text{carbon atoms})}$ are ~1.257×10^{-15} m^2, ~5.239×10^{-20} m^2 and ~47976, respectively. Thus, we found that the number of amino groups on the surface of GEMNPs-50 Torr (i.e., ~3.22×10^5) is about 6.7 times higher than the number of carbon atoms on the outmost layer of one nanoparticle (i.e., ~47976). This can be attributed to the fact that these covers are mainly composed of nitrogen doped substituent groups with relatively high molecular weights, which will provide much more free bonds to link amino groups. However, the further study will be needed to explain the present experimental results by cross-checking using other methods, such as Nuclear Magnetic Resonance (NMR) measurement or XPS analysis. Whereas the parallel graphite layers are not affected by the different working pressures, because they are formed by re-precipitated carbon atoms from metallic matrix rather than from dissociated CH_4/NH_3 species.

As reported in our previous papers, the plasma functionalized GEMNPs had a highly efficient bioconjugation property by using biotin–avidin system [38]. The amino group-functionalized GEMNPs were served to immobilize with an *Escherichia coli* (*E.coli*) antibody on their surfaces and incubated with *E.coli* bacteria further [39]. The antibody-integrated magnetic beads have also been functionalized for *influenza* A virus capture [40]. Through a plasma-induced method, we synthesized chitosan-grafted magnetic bentonite and carboxymethyl cellulose-grafted magnetic bentonite which showed a good magnetic properties and significant adsorption capacities for the enrichment of radionuclides [4,41]. Bystrzejewski et al. investigated carbon-coated magnetic nanoparticles as mobile adsorbents to remove heavy metal ions (Cu^{2+}, Co^{2+}, Cd^{2+}) from aqueous solutions, which had considerably higher adsorption capacities than those of activated carbons [42]. Niu et al. have prepared core/shell structured carbon-encapsulated magnetic nanoparticles using inorganic iron salt and glucose solution as precursor substance. These nanocomposites exhibited a high enrichment for various organic compounds including bisphenol A, 4-n-nonylphenol, 4-tert-octylphenol, etc [43]. Therefore, GEMNPs are versatile nanomaterials which can be functionalized with various types of functional groups and active molecules to exhibit numerous potentials in environmental pollution management and biomedical applications.

4. Conclusions

In this study, a versatile one-step DC arc discharge method was applied to fabricate GEMNPs functionalized by a large amount of amino groups uniformly in the working gas mixture of $He/CH_4/NH_3$. By changing the molar ratio of NH_3 from 0% to 5.0% and the working gas pressures from 25 Torr to 100 Torr, different numbers of modified amino groups are quantitatively confirmed by the chemical derivatization method. The optimized condition of this one-step fabrication process for the effective functionalization of amino groups is achieved. It shows that at 50 Torr with 0.1% of NH_3, amino groups are fully functionalized on the surface with a number of ~3.22×10^5 per nanoparticle. The surface structural integrity of outmost layers of GEMNPs increases as the molar ratio of NH_3 decreases from 1.0% to 0.1%. The adding NH_3 not only provides -NH or $-NH_2$ fragment species to introduce amino groups incorporating with the dangling bonds activated by H radicals, but also performs the construction of networks to flatten the surfaces of GEMNPs. This present work suggests that a one-step arc discharge method is desirable and easily controllable for the fabrication of amino-functionalized GEMNPs while maintaining their original bulk structures, which can be also used to synthesize other metallic nanoparticles efficiently for various applications.

Acknowledgements

This work was supported in part by Grant-in-Aid for Scientific Research (No. 25246029, 16K13709) from the Japan Society for the Promotion of Science.

References

[1] S. Mornet, S. Vasseur, F. Grasset, P. Verveka, G. Goglio, A. Demourgues, et al., Magnetic nanoparticle design for medicine applications, Prog. Solid State Chem. 34 (2–4) (2006) 237–247.
[2] A.H. Lu, W. Schmidt, N. Matoussevitch, H. Bönnermann, B. Spliethoff, B. Tesche, et al., Nanoengineering of a magnetically separable hydrogenation catalyst, Angew. Chem. Int. Ed. 43 (33) (2004) 4303–4306.
[3] A.K. Gupta, M. Gupta, Synthesis and surface engineering of iron oxide nanoparticles for biomedical applications, Biomaterials 26 (18) (2005) 3995–4021.
[4] R. Hu, X. Ren, G. Hou, D. Shao, Y. Gong, X. Chen, et al., A carboxymethyl cellulose modified magnetic bentonite composite for efficient enrichment of radionuclides, RSC Adv. 6 (2016) 65136–65145.
[5] T. Hyeon, Chemical synthesis of magnetic nanoparticles, Chem. Commun. 21 (8) (2003) 927–934.
[6] S. Chikazumi, S. Taketomi, M. Ukita, M. Mizukami, H. Miyajima, M. Setogawa, et al., Physics of magnetic fluids, J. Magn. Magn. Mater. 65 (2–3) (1987) 245–251.
[7] Y. Kobayashi, M. Horie, M. Konno, B. Rodriguez-Gonzalez, L.M. Liz-Marzan, Preparation and properties of silica-coated cobalt nanoparticles, J. Phys. Chem. B 107 (30) (2003) 7420–7425.
[8] J. Liu, S.Z. Qiao, Q.H. Hu, G.Q. Lu, Magnetic nanocomposites with mesoporous structures: synthesis and applications, Small 7 (4) (2011) 425–443.
[9] A.H. Lu, W. Li, N. Matoussevitch, B. Spliethoff, H. Bönnemann, F. Schüth, Highly stable carbon-protected cobalt nanoparticles and graphite shells, Chem. Commun. 1 (2005) 98–100.
[10] L.E. Euliss, S.G. Grancharov, S. O'Brien, T.J. Deming, G.D. Stucky, C.B. Murray, et al., Cooperative assembly of magnetic nanoparticles and block copolypeptides in aqueous media, Nano Lett. 3 (11) (2003) 1489–1493.
[11] M. Kim, Y. Chen, Y. Liu, X. Peng, Super-stable, highly-quality Fe_3O_4 dendron-nanocrystals dispersible in both organic and aqueous solutions, Adv. Mater. 17 (11) (2005) 1429–1432.
[12] G.X. Zhu, X.W. Wei, C.J. Xia, Y. Ye, Solution route to single crystalline dendritic cobalt nanostructures coated with carbon shells, Carbon 45 (6) (2007)

1160–1166.
[13] J. Liu, N.P. Wickramaratne, S.Z. Qiao, M. Jaroniec, Molecular-based design and emerging applications of nanoporous carbon spheres, Nat. Mater. 14 (2015) 763–774.
[14] L. Wang, J. Bao, L. Wang, F. Zhang, Y. Li, One-pot synthesis and bioapplication of amine-functionalized magnetite nanoparticles and hollow nanospheres, Chem. Eur. J. 12 (24) (2006) 6341–6347.
[15] L.Z. Gao, J.M. Wu, S. Lyle, K. Zehr, L.L. Cao, D. Gao, Magnetite nanoparticle-linked immunosorbent assay, J. Phys. Chem. C 112 (44) (2008) 17357–17361.
[16] E.E. Carpenter, C.T. Seip, C.J. O'Connor, Magnetism of nanophase metal and metal alloy particles formed in ordered phases, J. Appl. Phys. 85 (8) (1999) 5184–5186.
[17] A. Bee, R. Massart, S. Neveu, Synthesis of very fine maghemite particles, J. Magn. Magn. Mater. 149 (1–2) (1995) 6–9.
[18] C. Chen, A. Ogino, X. Wang, M. Nagatsu, Plasma treatment of multiwall carbon nanotubes for dispersion improvement in water, Appl. Phys. Lett. 96 (2010) 131504.
[19] T.E. Saraswati, A. Ogino, M. Nagatsu, Plasma-activated immobilization of biomolecules onto graphite-encapsulated magnetic nanoparticles, Carbon 50 (3) (2012) 1253–1261.
[20] E.B. Yang, S. Tsumura, M. Nagatsu, Surface properties of plasma-functionalized graphite-encapsulated gold nanoparticles prepared by a direct current arc discharge method, J. Phys. D. Appl. Phys. 49 (18) (2016) 185304.
[21] T.E. Saraswati, S. Tsumura, M. Nagatsu, High-efficiency plasma surface modification of graphite-encapsulated magnetic nanoparticles using a pulsed particle explosion technique, Jpn. J. Appl. Phys. 53 (1) (2014) 010205.
[22] J. Carlsson, H. Drevin, R. Axén, Protein thiolation and reversible protein-protein conjugation. N-Succinimidyl 3-(2-pyridyldithio)propionate, a new heterobifunctional reagent, Biochem. J. 173 (3) (1978) 723–737.
[23] G. Hermanson, Bioconjugate Techniques, second ed., Academic Press, New York, 2008, p. 277.
[24] X.L. Dong, Z.D. Zhang, Q.F. Xiao, X.G. Zhao, Y.C. Chuang, S.R. Jin, et al., Characterization of ultrafine γ-Fe(C), α-Fe(C) and Fe_3C particles synthesized by arc-discharge in methane, J. Mater. Sci. 33 (7) (1998) 1915–1919.
[25] P. Balaz, Mechanochemistry in Nanoscience and Minerals Engineering, Springer, Berlin, 2008.
[26] A.N. Bhoj, M.J. Kushner, Repetitively pulsed atmospheric pressure discharge treatment of rough polymer surfaces: II. Treatment of micro-beads in $He/NH_3/H_2O$ and $He/O_2/H_2O$ mixtures, Plasma Sources Sci. Technol. 17 (3) (2008) 035025.
[27] S.J. Kang, V.M. Donnelly, Optical absorption and emission spectroscopy studies of ammonia-containing plasmas, Plasma Sources Sci. Technol. 16 (2) (2007) 265–272.
[28] R. Hu, M.A. Ciolan, X.K. Wang, M. Nagatsu, Copper induced hollow carbon nanospheres by arc discharge method: controlled synthesis and formation mechanism, Nanotechnology 27 (33) (2016) 335602.
[29] A. Ogino, S. Noguchi, M. Nagatsu, Optimization of amino group introduction onto polyurethane surface using ammonia and argon surface-wave plasma, Jpn. J. Appl. Phys. 50 (8) (2011) 08JF06.
[30] V.V. Kovalevski, A.N. Safronov, Pyrolysis of hollow carbons on melted catalyst, Carbon 36 (7–8) (1998) 963–968.
[31] J. Jiao, S. Seraphin, Single-walled tubes and encapsulated nanoparticles: comparison of structural properties of carbon nanoclusters prepared by three different methods, J. Phys. Chem. Solids 61 (7) (2000) 1055–1067.
[32] Y. Saito, Y. Tani, A. Kasuya, Diameters of single-wall carbon nanotubes depending on helium gas pressure in an arc discharge, J. Phys. Chem. B 104 (11) (2000) 2495–2499.
[33] D. Kasuya, T. Ishigaki, T. Suganuma, Y. Ohtsuka, S. Suzuki, H. Shiromaru, et al., HPLC analysis for fullerenes up to C_{96} and the use of the laser furnace technique to study fullerene formation process, Eur. J. Phys. D. 9 (1) (1999) 355–358.
[34] P.S. Raghavan, Concepts and Problems in Inorganic Chemistry, Discovery Publishing House, New Delhi, 1998.
[35] D. Zhou, Y. Cui, P. Xiao, M. Jiang, B. Han, A general and scalable synthesis approach to porous graphene, Nat. Commun. 5 (2014) 4716.
[36] Y. Saito, T. Yoshikawa, M. Okuda, N. Fujimoto, Iron particles nesting in carbon cages grown by arc discharge, Chem. Phys. Lett. 212 (3–4) (1993) 379–383.
[37] L. Lin, S. Zhang, Creating high yield water soluble luminescent graphene quantum dots via exfoliating and disintegrating carbon nanotubes and graphite flakes, Chem. Commun. 48 (2012) 10177–10179.
[38] A. Viswan, H. Chou, A. Sakudo, M. Nagatsu, Bioconjugation efficiency of plasma-functionalized carbon-encapsulated iron nanoparticles with biotin-avidin system, Biomed. Phys. Eng. Express 1 (4) (2015) 045104.
[39] A. Viswan, H. Chou, K. Sugiura, M. Nagatsu, Surface modification of graphite-encapsulated iron nanoparticles by RF excited Ar/NH_3 gas mixture plasma and their application to *Escherichia coli* capture, J. Phys. D. Appl. Phys. 49 (36) (2016) 364001.
[40] A. Sakudo, H. Chou, K. Ikuta, M. Nagatsu, Integration of antibody by surface functionalization of graphite-encapsulated magnetic beads using ammonia gas plasma technology for capturing *influenza* A virus, Bioorg Med. Chem. Lett. 25 (9) (2015) 1876–1879.
[41] S. Yang, N. Okada, M. Nagatsu, The highly effective removal of Cs^+ by low turbidity chitosan-grafted magnetic bentonite, J. Hazard Mater 301 (2016) 8–16.
[42] M. Bystrzejewski, K. Pyrzyńska, A. Huczko, H. Lange, Carbon-encapsulated magnetic nanoparticles as separable and mobile sorbents of heavy metal ions from aqueous solutions, Carbon 47 (4) (2009) 1201–1204.
[43] H. Niu, Y. Wang, X. Zhang, Z. Meng, Y. Cai, Easy synthesis of surface-tunable carbon-encapsulated magnetic nanoparticles: adsorbents for selective isolation and preconcentration of organic pollutants, ACS Appl. Mater. Interfaces 4 (1) (2012) 286–295.